

High-Resolution Phase Doppler Particle Sizing based on Hilbert Transform Signal Processing

Peter Lehmann, E. Hanno Schombacher, Thomas Wriedt*

(Received: 22 May 1995)

Abstract

A new phase Doppler anemometry (PDA) signal processing method based on a Hilbert transform algorithm is introduced and analysed. By generating a 90° phase-shifted burst signal in the time domain, the envelope of the Doppler burst can be determined. In addition, this envelope is approximated by a Gaussian exponential function. The difference of the maxima of these Gaussian approximations for two related PDA bursts gives an estimate of the time difference between these time-shifted signals. With the introduction of this estimation

method, the restriction to the $[0,360^\circ]$ interval resulting from conventional signal analysis may be avoided in many cases. To investigate the dependence on SNR, burst position, burst frequency and sampling rate, results of computer simulations are presented. The feasibility of the method is demonstrated briefly by experimental results. Phase differences of more than 2000° arising from the measurement of monodisperse droplets by a conventional PDA setup could be determined.

1 Introduction

During the last decade, phase Doppler anemometry (PDA) has become a well-established method for particle and droplet size characterization. The PDA principle is based on the relationship between the measured phase difference of two burst signals detected under different elevation angles and the diameter of a spherical particle passing the measuring volume. The parameters of a PDA setup are generally chosen in such a way that a linear relationship between the phase difference $\Delta\Phi$ and the particle diameter occurs [1,2].

Nowadays, PDA and LDA signal processing is mostly based on the fast Fourier transform (FFT) since the FFT algorithm works well even in cases of low signal-to-noise ratios (SNR), such as -5 dB [7,14,16]. Digital signal processors were developed which allow low-cost real-time signal processing by spectrum analysis in LDA and PDA applications [5,13].

However, phase differences may be determined within the range 0 – 360° using two detectors only. Therefore, particle diameters from 0 to ∞ are sorted into this $[0,360^\circ]$ interval. If, for example, the particle diameter leads to a phase difference of 400° for a PDA setup with given geometrical parameters, the measured particle diameter is calculated assuming a phase difference of 40° . Of course, it is possible to avoid this problem by choosing specific geometrical parameters for the setup (for example, small elevation angles) which lead to real phase differences of less than 360° even for the largest analysed particles. However, this approach does not allow the determination of particle diameter distributions with high resolution. In order to obtain high resolved size distributions, several modified PDA arrangements were proposed. One possibility is to use a PDA setup with three detectors measuring three burst signals at different elevation angles [10]. Comparing the

different phase differences, the real particle diameter may be determined with higher resolution but nevertheless the measuring range is restricted. A new method in this context is the dual-mode PDA proposed by Tropea et al. [15]. Here, a conventional PDA setup is combined with a planar PDA arrangement using a second wavelength of light. Besides its advantages with respect to trajectory and slit effects, this method is also well suited to avoiding the problem concerning the $[0,360^\circ]$ measuring range. From the different theoretical phase difference to diameter calibration curves of the dual-mode arrangement, the real diameter may be obtained even in cases in which the diameter leads to phase differences of more than 360° for the conventional PDA setup. However, both methods require much expense in technical equipment and have a restricted measuring range.

A method to determine phase differences of more than 360° using signal processing based on correlation techniques was proposed by Borys [3]. For this method, high-quality burst signals of more than 10 dB SNR are necessary even if the signals are sampled by 512 sampling values.

In this paper, a signal processing method based on a Hilbert transform algorithm is proposed. The Hilbert transform is used to obtain a 90° phase-shifted burst signal. From the measured burst data and the 90° phase-shifted data, the square of the burst envelope is estimated as the absolute square of the complex amplitudes. Using a least-squares method, this estimated envelope is approximated by a Gaussian exponential function due to the spatial intensity distribution of a laser beam in the TEM_{00} mode. From the difference in the maxima of such Gaussian approximations for two PDA bursts, an estimate of the time difference between the time-shifted PDA signals is obtained. This estimate may be used to validate the phase difference obtained by FFT signal analysis. The method will yield reliable results even in cases of low SNR. Signal processing according to this method may be carried out by software implementation and therefore it does not require any further hardware.

* Dr.-Ing. P. Lehmann, Dipl.-Ing. E. H. Schombacher, Dr.-Ing. T. Wriedt, University of Bremen, Meß- und Regelungstechnik/Verfahrenstechnik, FB4, Postfach 330440, D-28334 Bremen (Germany).

2 Hilbert Transform Envelope Estimation

Generally, PDA bursts are sampled by N sampling values which correspond to time values $n\Delta t$, with $n \in \{0, \dots, N-1\}$, $N = 2^{m_0}$ where m_0 is an integer and $m_0 \geq 2$. The real signal values $s_n = s(n\Delta t)$ are processed by an FFT algorithm which carries out the discrete Fourier transform (DFT)

$$s_k = S(k\Delta f) = \sum_{n=0}^{N-1} s(n\Delta t) \exp(-i2\pi kn/N), \quad (1)$$

with a frequency resolution of $\Delta f = 1/(N\Delta t)$ and $i = \sqrt{-1}$. The Fourier transform S_k , $k \in \{0, \dots, N-1\}$ is complex valued with the real part $\text{Re}\{S_k\}$ and the imaginary part $\text{Im}\{S_k\}$:

$$S_k = \text{Re}\{S_k\} + i \text{Im}\{S_k\}.$$

Obviously, in the case of a sinusoidal signal with frequency f_o the frequency $j_o = f_o/\Delta f$ in terms of DFT spectral lines corresponds to the number of periods of the signal within the sampled time range $N\Delta t$:

$$j_o = \frac{f_o}{\Delta f} = \frac{N\Delta t}{T_0} \quad (2)$$

with the period $T_0 = 1/f_o$ of the signal.

The negative frequency values are represented by $k\Delta f$, with $k \in \{N/2, \dots, N-1\}$. Since these negative frequency values do not have any physical merit, the Fourier transform values are restricted to positive frequencies by the transform:

$$A_k = \begin{cases} 2S_k & 0 < k < N/2 \\ S_k & k = 0 \\ 0 & k \geq N/2. \end{cases} \quad (3)$$

In addition, transforming A_k to the time domain by inverse FFT leads to the analytical time signal $a_n = a(n\Delta t)$:

$$a_n = \text{Re}\{a_n\} + i \text{Im}\{a_n\} = \frac{1}{N} \sum_{k=0}^{N-1} A_k \exp(i2\pi kn/N) \quad (4)$$

with $\text{Re}\{a_n\} = s_n$ and $n \in \{0, \dots, N-1\}$. Thus, the imaginary part $\text{Im}\{a_n\}$ is obtained from the real part $\text{Re}\{a_n\}$ by the so-called Hilbert transform. The square envelope e_n of the actual time-dependent signal s_n is given by [8]

$$e_n = (\text{Re}\{a_n\})^2 + (\text{Im}\{a_n\})^2 = |a_n|^2. \quad (5)$$

These relationships become more obvious by assuming a sinusoidal signal $s_n = \sin(2\pi N_0 n/N)$ with $N_0 \in \{1, \dots, N/2-1\}$. In this case it follows that

$$A_k = \begin{cases} \frac{N}{i} & \text{for } k = N_0 \\ 0 & \text{for } k \neq N_0. \end{cases}$$

Therefore, we obtain $a_n = (1/i) \exp(i2\pi N_0 n/N)$ and $e_n = a_n a_n^* = 1$.

2.1 Gaussian Approximation by Least Squares

As shown in Section 3, the empirical envelope e_n of the burst signal is sensitive to noise. Therefore, a least-squares fitting

algorithm [4] is used in order to detect a representative maximum value of the burst envelope. The time-discrete function $e_n = e(n\Delta t)$, with $n \in \{0, \dots, N-1\}$, will be approximated by a continuous Gaussian function:

$$g(t) = \beta \exp\left(-\frac{(t-\tau)^2}{\sigma^2}\right) \quad (6)$$

$$\Leftrightarrow \ln(g(t)) = \ln(\beta) - \frac{(t-\tau)^2}{\sigma^2} \quad (7)$$

$$= b_0 + b_1 t + b_2 t^2, \quad (8)$$

with $b_0 = \ln(\beta) - (\tau^2/\sigma^2)$, $b_1 = \tau/\sigma^2$, $b_2 = 1/\sigma^2$. This Gaussian shape of the envelopes arises from the spatial intensity distribution of a laser beam in the TEM₀₀ mode. After having applied the logarithm function in Eq. (7), only a quadratic interpolation has to be performed in order to evaluate b_0 , b_1 and b_2 .

According to the least-squares method [4], three linear equations which contain the three unknown parameters b_0 , b_1 and b_2 must be solved:

$$b_0(n_{\max} - n_{\min} + 1) + b_1[t] + b_2[t^2] = [f], \quad (9)$$

$$b_0[t] + b_1[t^2] + b_2[t^3] = [tf], \quad (10)$$

$$b_0[t^2] + b_1[t^3] + b_2[t^4] = [t^2 f], \quad (11)$$

where we have assumed

$$(n_{\min} \Delta t)^m + ((n_{\min} + 1) \Delta t)^m + \dots + (n_{\max} \Delta t)^m = [t^m], \quad (12)$$

$$(n_{\min} \Delta t)^m f_{n_{\min}} + ((n_{\min} + 1) \Delta t)^m f_{n_{\min} + 1} + \dots + (n_{\max} \Delta t)^m f_{n_{\max}} = [t^m f] \quad (13)$$

and $f_n = \ln e_n$ with $n \in \{0, \dots, N-1\}$.

Assuming a threshold e_{\min} , the values of n_{\min} and n_{\max} are computed by fulfilling the condition

$$e_n > e_{\min} \text{ for } n \in \{n_{\min}, n_{\min} + 1, \dots, n_{\max}\}.$$

This condition makes the procedure robust versus noise phenomena. According to Eqs. (9)–(11), the parameters b_0 , b_1 and b_2 may be calculated easily. Using the relationships

$$\sigma = \frac{1}{\sqrt{b_2}}, \quad \tau = \frac{b_1 \sigma^2}{2} \text{ and } \beta = \exp\left(b_0 + \frac{\tau^2}{\sigma^2}\right)$$

the parameters of the Gaussian function $g(t)$ of Eq. (6) are defined with τ as the maximum position of this function.

The complete procedure is carried out for both PDA burst signals. The difference $\Delta\tau = \tau_2 - \tau_1$ of the maximum position τ_1 of the temporally first burst signal and τ_2 of the second burst signal is used as an estimate of the time difference ΔT between the two bursts.

3 Computer Simulations

In this section, computer simulations which were performed in order to study the feasibility and the reliability of the new method will be outlined. In this context, especially the SNR dependence of the time shift estimation is relevant.

A noise generation procedure was realized based on an algorithm proposed by *Kafadar* [6] using a pseudo random number generator described by *Park and Miller* [9]. Gaussian white noise was generated and added to the simulated burst signal data assuming a specific SNR value given by the time domain definition

$$SNR = 10 \log_{10} \left(\frac{\text{mean square of signal}}{\text{variance of noise}} \right),$$

where the signals were Gaussian weighted sinusoids and the noise bandwidth was equal to the Nyquist frequency [12].

Figure 1a shows the absolute square of simulated laser Doppler signal which lies symmetrically within the sampled data window. The number N of sampling values was 128 and an SNR of 40 dB was assumed. The envelope estimation which results from the Hilbert transform procedure is plotted as a dotted line in Figure 1b. The solid line in Figure 1b gives the signal envelope obtained by the Gaussian least-squares fitting. Since the quality of the signal is high there are only small deviations between the two sets of results in Figure 1b. In Figure 2 the same curves are plotted but in this case only 10 dB was chosen as the SNR value. The deviations between the two envelope estimates in Figure 2b are striking. Obviously, for low SNR values the maximum position of the burst signal may be determined from the Gaussian approximation only. Figure 3 was obtained for a simulated 10 dB laser-Doppler signal which has a non-symmetrical position within the sampled time range. Even in this case the maximum position is reproduced satisfactorily by the Gaussian envelope estimation. Further investigations concern the “rate of validation” of PDA signals assuming phase differences of more than 360° . The “rate of validation” is defined as follows: when the phase difference is determined correctly by the $m \cdot 360^\circ$ phase shift of the Gaussian approximation envelope plus the value $\Delta\Phi$ obtained by conventional FFT signal analysis, the result will be validated. This means that the condition

$$|m \cdot 360^\circ + \Delta\Phi - 360^\circ \cdot \Delta\tau f_0| = \text{minimum}$$

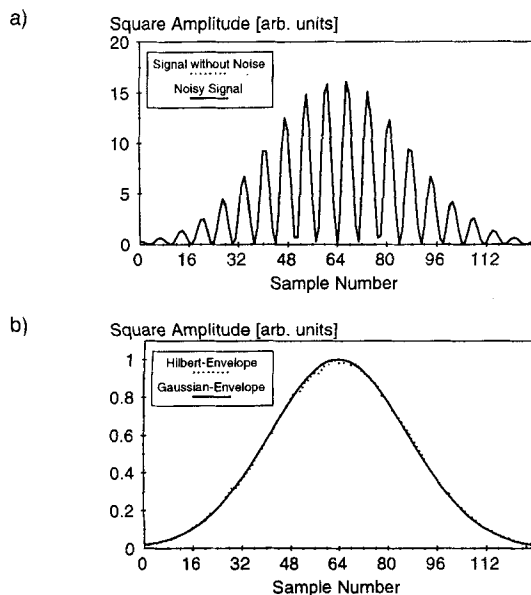


Fig. 1: Amplitude absolute square and envelope approximation for a simulated burst signal. Maximum position, 64; $1/e^2$ width, 64; SNR, 40 dB.

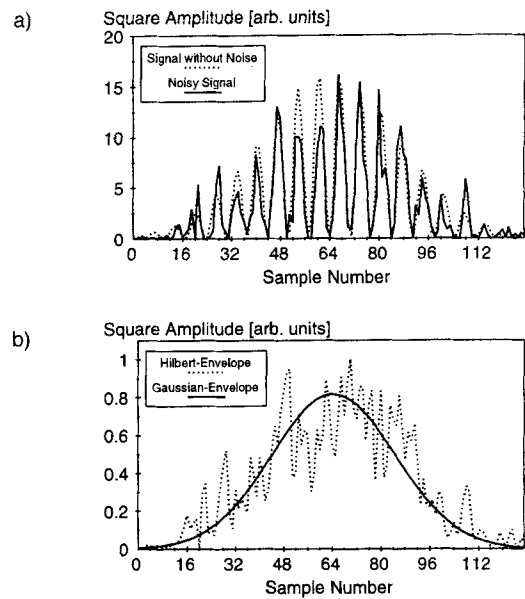


Fig. 2: Amplitude absolute square and envelope approximation for a simulated burst signal. Maximum position, 64; $1/e^2$ width, 64; SNR, 10 dB.

has to be proved for several integers m in order to obtain the correct m value. For the following simulation results a phase difference of 400° was assumed.

The accuracy of the envelope maximum estimation does not depend on the signal frequency. Consequently, the rate of validation decreases strongly with an increasing number of interference fringes within the measuring volume and therefore with the number j_0 of periods within the sampled time range. This dependence is plotted in Figure 4a for SNR values of 5, 10 and 15 dB. The ordinate in Figure 4 is scaled in terms of the normalized frequency j_0 according to Eq. (2). For each SNR value 1000 pairs of burst signals were simulated. Even in the case of a 5 dB SNR a nearly 100% validation for frequency values between 5 and 10 of 64 FFT spectral lines can be

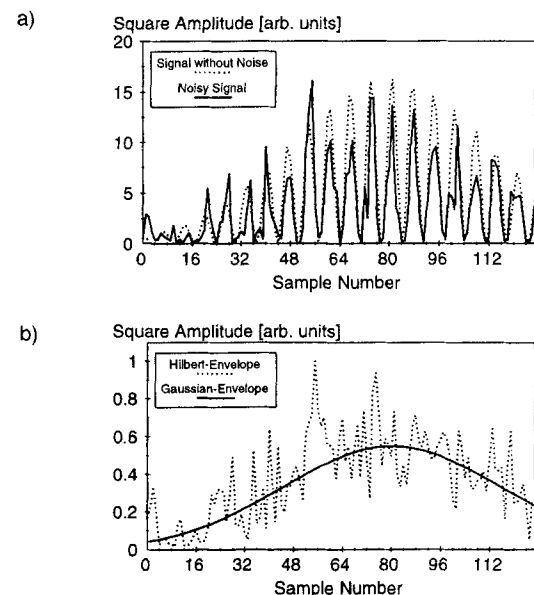


Fig. 3: Amplitude absolute square and envelope approximation for a simulated burst signal. Maximum position, 80; $1/e^2$ width, 90; SNR, 10 dB.

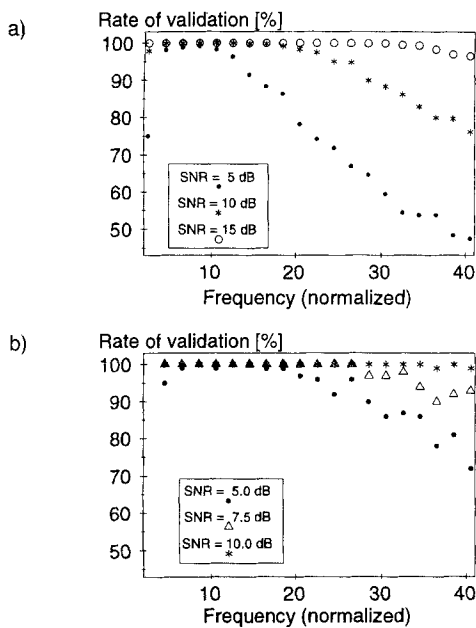


Fig. 4: Rate of validation for several SNR values. (a) $N = 128$; maximum position (burst 1), 64; $1/e^2$ width, 64. (b) $N = 512$; maximum position (burst 1), 256; $1/e^2$ width, 256; $\Phi_{12} = 400^\circ$.

obtained. With an increasing SNR value this range becomes broader until for SNR values of more than 20 dB the rate of validation reaches 100% for all frequency values of interest.

In Figure 5a, the rate of validation is plotted versus SNR for different numbers of burst periods within the sampled range. The first case assumes that only 6.5 signal periods are sampled while the particle passes the PDA measuring volume. In this case a validation rate of nearly 100% is reached for SNR values of more than 5 dB. Even for an SNR of only -5 dB the rate of validation is more than 50%. Assuming 20.5 signal periods, a 100% validation is possible only for SNRs of more than 12 dB. Since this phenomenon depends on the sample number per

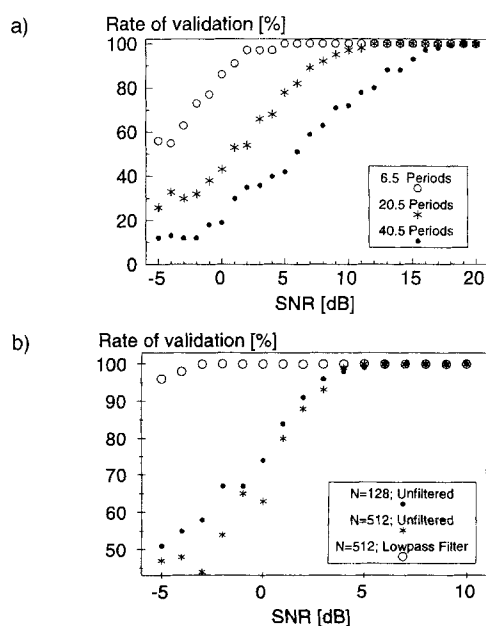


Fig. 5: (a) SNR-dependent rate of validation for several burst frequencies, $N = 128$. (b) Improvement of the rate of validation by low-pass filtering assuming $N\Delta t/T_0 = 9.5$.

period, we conclude that a broader range of 100% validation may be reached by sampling the PDA signal with a higher sampling rate. The results plotted in Figure 4b are analogous to those in Figure 4a but in this case 512 sampling values were chosen. Comparing the curves obtained for equal SNR values, the above-mentioned effect becomes obvious.

A further improvement was achieved by low-pass filtering the Fourier transformed signal data. Results for a constant number of 9.5 periods within the data window are shown in Figure 5b. The rates of validation computed for 128 and 512 sampling values do not show significant deviations. Improved rates of validation arise by computing the spectral line j_0 by FFT and defining according to Eq. (3): $A_k = 0$ even for $k \leq j_0 + 4$. In this case a rate of validation of 100% was reached for SNR values down to -3 dB. This effect is primarily caused by the assumption of white noise. Since the high-frequency part of the PDA signal is restricted to frequency values of a few spectral lines more than the maximum spectral line, the high-frequency noise contributions may be eliminated easily by low-pass filtering.

In the following, the term “non-weighted phase difference estimation” will describe the method of sorting each pair of PDA burst signals within a 360° interval by means of the envelope estimation and using the phase difference value obtained by FFT signal analysis to determine the phase difference accurately within this interval. Obviously, this method requires an accurate envelope estimation. Nevertheless, in most practical PDA applications, not particle sizes corresponding to unique events but size distributions of particle ensembles are of interest. In all these cases, a 100% validation is not necessary if a total width of a corresponding phase difference distribution of less than 360° can be assumed. Then, using the method introduced in this paper, a distribution of the time shifts of PDA bursts can be obtained by counting the corresponding events for several neighbouring 360° intervals.

Determining the centre of such distributions will yield an estimate $\tilde{\Phi}_{12}$ for the real absolute phase difference Φ_{12} . By sorting the FFT phase differences $\Delta\Phi$ for each pair of bursts assuming that the condition

$$|m \cdot 360^\circ + \Delta\Phi - \tilde{\Phi}_{12}| = \text{minimum}$$

with an integer m is fulfilled, the absolute phase difference distribution and therefore the real size distribution can be obtained as shown in the next section. This principle called “weighted phase difference estimation” will work even for rates of validation of less than 50%.

4 Experimental Investigations

To test the capability of the Hilbert transform envelope estimation under experimental conditions, phase Doppler measurements were performed at a flow of monodisperse droplets of toluene in water.

The physical background of the phase Doppler measurement technique has been explicitly discussed in the literature (e.g. [1, 2]). The PDA setup used for the purpose of this study is illustrated in Figure 6. The PDA-transmitting system consisted of 40 mW diode laser ($\lambda = 830$ nm) and a conventional optical PDA arrangement (beam splitter, polarizers and collimator lens). As receiving unit a one-lens system integrating two

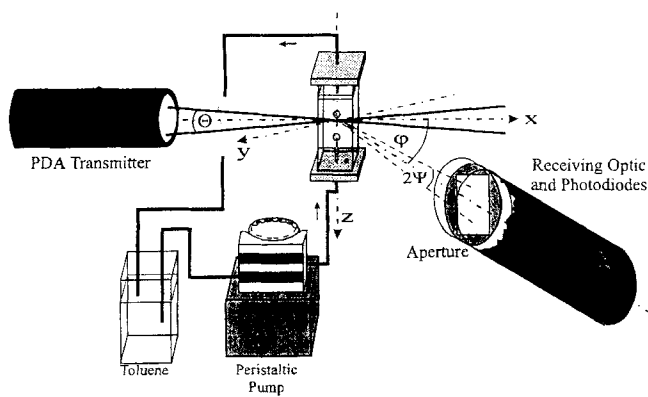


Fig. 6: Experimental PDA setup.

avalanche photodiodes in one casing was used. By applying receiving lenses of different focal length and apertures of different width, the detector elevation angle Ψ and consequently the measuring range of the PDA setup, which is defined by the maximum droplet diameter that can be sorted into the $[0, 360^\circ]$ interval, could be varied. In this context, an increasing value of Ψ causes a decreasing particle size measuring range.

For each burst signal, a threshold of 10 dB was used as the minimum SNR value. The burst signals were sampled by 128 sampling points, digitized with 8 bits and stored for further signal processing. As verification of the PDA size measurements, the droplets were observed by a microscope and recorded by a CCD camera and a video tape recorder, which allowed off-line size analysis by digital image processing.

The physical and chemical properties of the liquid-liquid system toluene-water ($n_{\text{rel}} = 1.122$) have been briefly described [11]. Based on light scattering considerations (Mie theory, geometrical optics), an off-axis angle φ of 15° giving first-order refracted light was considered a good choice in order to obtain a linear relationship between the diameter of the spherical particle and the total phase difference of the Doppler bursts received by the two photodetectors. This is an important prerequisite for correct size determination by PDA. As illustrated in Figure 6, the experimental chamber consisted of a rectangular cell ($20 \times 20 \times 100$ mm) of optical glass with the bottom and top made of stainless steel. By means of a peristaltic pump, a steady-state flow of monodisperse toluene droplets (in all cases 2.47 mm diameter) could be produced at the top of a hypodermic needle. Since the PDA measurement is sensitive to droplet trajectory effects, the cell could be adjusted in all axes by means of a 3D micrometer traverse table.

The results of the first series of measurements ($\Psi = 0.57^\circ$) are plotted in Figure 7a–c. The number of signal periods within the sampled range was about 14. The distributions obtained by conventional, FFT-based signal processing (a) are compared with the distributions calculated by the non-weighted phase difference estimation (b) and the weighted estimation (c) using the estimate $\hat{\Phi}_{12}$. The maximum of the phase difference distribution in Figure 7a is established in the $[0, 360^\circ]$ interval at 95° , whereas in Figure 7b the distribution is shifted to the second 360° interval and has a maximum value at 455° . This classification corresponds to the phase shift which can be predicted by geometrical optics [1] for the PDA arrangement used in this case. As some of the measured phase differences are sorted into different 360° intervals by the envelope estimation

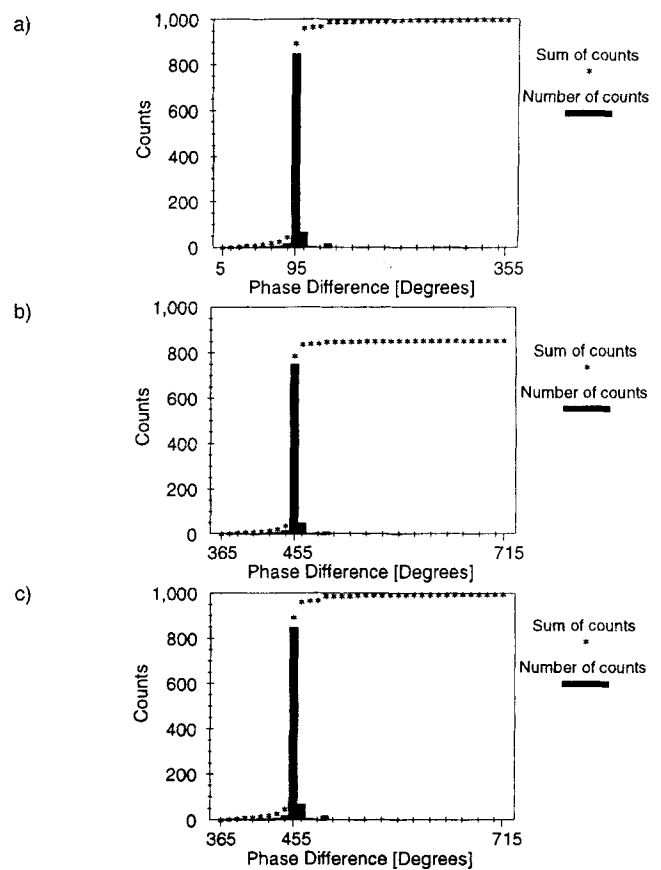


Fig. 7: Phase difference distributions for a phase difference mean value of 455° : (a) resulting from FFT signal processing; (b) using the non-weighted phase difference estimation method; and (c) using the weighted phase difference estimation method.

algorithm (see Table 1), the maximum peak of the distribution is not as distinctive as it is in the first case (Figure 7a).

A pronounced improvement can be achieved by the weighted phase difference estimation (Figure 7c). In this case an estimate $\hat{\Phi}_{12}$ was obtained. The centre of the phase difference distribution (between -800° and 2800°) which was obtained by the Gaussian approximation method (Table 1) is used to estimate the mean value $\hat{\Phi}_{12} = 418^\circ$. If the real phase difference distribution is broader, a more accurate mean phase difference estimation may be realized by subdividing the phase difference axis into smaller intervals. For example, according to the non-weighted phase difference distributions in Figure 7b, any mean value estimation will be close to the real phase difference mean values.

The advantage of the weighted phase difference estimation method is even more obvious in the second series of measurements ($\Psi = 2.23^\circ$) illustrated in Figure 8a–c, where the number of sampled burst periods was about 18. In this case the distribution obtained by conventional FFT signal processing is split (Figure 8a). The peak is to be found 5° to the left side of the $[0, 360^\circ]$ interval. A second small peak appears at the end of the interval at 355° .

The distribution resulting from the Gaussian phase difference estimation according to Table 1 (second series) is plotted in Figure 8b. As expected from geometrical optics [1], the maximum peak of the distribution is shifted to the sixth 360° interval. Additionally, the distribution is spread over many 360° intervals from 360° to 3600° .

At first glance, the results in Figures 8a and 8b seem to

Table 1: Sorting of phase differences estimated by the Gaussian approximation method to 360° intervals.

First series										
interval (degrees)	-800	-440	-80	280	640	1000	1360	1720	2080	2440
	to	to	to	to	to	to	to	to	to	to
	-440	-80	280	640	1000	1360	1720	2080	2440	2800
counts	1	3	121	862	7	3	0	0	0	0
Second series										
interval (degrees)	180	540	900	1260	1620	1980	2340	2700	3060	3420
	to	to	to	to	to	to	to	to	to	to
	540	900	1260	1620	1980	2340	2700	3060	3420	3780
counts	8	13	39	123	195	237	141	116	68	25

contradict the PDA measurement of monodisperse size distributed droplets. Actually, since the parameters are critical in this case, the Gaussian approximation method does not work accurately and the estimated time shift $\Delta\tau$ shows large variations. In addition, the mean value of the distribution (2170°) is close to the border of two related 360° intervals and therefore ambiguities in the assignment of $\Delta\Phi$ values appear. Consequently, the phase differences $\Delta\Phi$ are not always sorted into the expected 360° interval by the envelope estimation (see Table I). This leads to displacements of the sorting which can be avoided by the weighted phase difference estimation method with an estimated mean value (Figure 8c). Using the FFT phase differences $\Delta\phi$ and the mean value of $\tilde{\phi}_{12} = 2170^\circ$ of the broad estimated time shift distribution of Table I (second series), a narrow monomodal distribution which now corresponds to the monodispersity of the droplets measured by PDA is obtained.

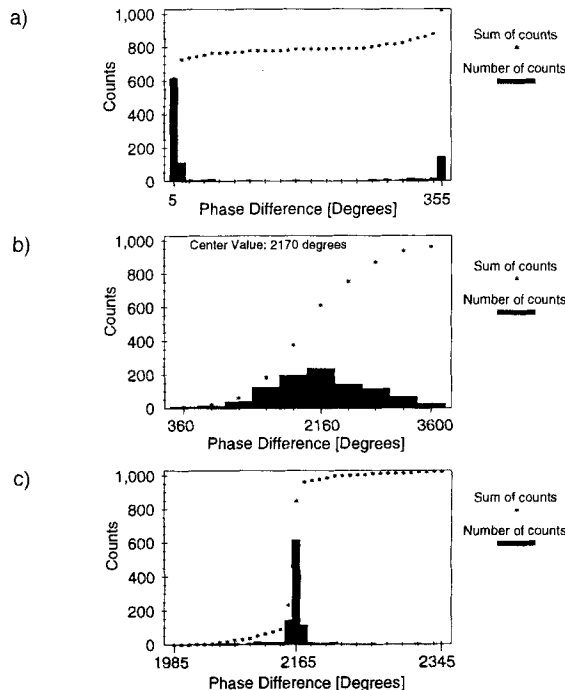


Fig. 8: Phase difference distributions for a phase difference mean value of 2165°: (a) resulting from FFT signal processing; (b) using the phase difference estimation obtained by Gaussian approximation according to Table I (second series); and (c) using the weighted phase difference estimation method.

5 Conclusions

A high-resolution PDA particle sizing method based on Hilbert transform signal processing was introduced and studied. An estimated phase difference value $\tilde{\Phi}_{12}$ is obtained from the time-shifted maximum positions of the estimated Gaussian envelopes of the PDA burst signals.

Estimated phase difference values were used to obtain phase difference distributions within the -1080° to $+3780^\circ$. However, high-quality signals or high sampling rates are required to reach close to 100% validation. Nevertheless, even for lower rates of validation the maximum of a real phase difference distribution may be determined with sufficient accuracy, as can be seen in Figures 7b and 8b.

Assuming that the total width of the real phase difference distribution is less than 360° , an accurate approximation of this distribution can be realized by sorting the phase differences resulting from FFT with respect to the mean phase difference $\tilde{\Phi}_{12}$ of the complete ensemble of events. Such weighted phase difference distributions are shown in Figures 7c and 8c.

This new method of post-processing PDA burst signals can yield particle diameter distributions of high resolution. In addition, a signal validation using the envelope information to distinguish between PDA bursts resulting from first-order refracted or reflected light can be implemented. This distinction will help to reduce measurement errors due to trajectory effects [15]. Furthermore, the envelope information can supply an estimation of signal intensity and the burst length.

Further studies will give more detailed information about the feasibility of the Hilbert transform envelope estimation method especially in terms of high resolution and improved validation of PDA results in spray experiments.

All numerical algorithms presented in this paper were realized by software implementation on microcomputers.

6 Symbols and Abbreviations

$a(t)$	analytical burst signal
a_n	nth sampling value of $a(t)$
a_n^*	complex conjugate of a_n
A_n	nth sampling value of the discrete Fourier transform of $a(t)$
b_0, b_1, b_2	parameters
β	normalization factor
Δf	frequency resolution
$\Delta\Phi$	phase difference value resulting from FFT

Δt	discretization time interval
ΔT	time difference between PDA bursts
$\Delta \tau$	time difference between estimated burst maximum positions
e_n	n th sampling value of the square envelope resulting from Hilbert transform
e_{\min}	envelope threshold
f_0	Doppler frequency
f_n	logarithm of the square envelope value e_n
$g(t)$	time-dependent Gaussian approximation
i	imaginary unit
$\text{Im}\{\dots\}$	imaginary part of the embraced expression
j_0	normalized Doppler frequency
k	index
λ	wavelength of light
m	integer
n	index
n_{\min}	integer, minimum value
n_{\max}	integer, maximum value
n_{rel}	relative refraction index
N	total number of sample points
N_0	number of periods
φ	off-axis angle
Φ_{12}	total phase difference
$\hat{\Phi}_{12}$	phase difference estimation
Ψ	elevation angle
$\text{Re}\{\dots\}$	real part of the embraced expression
$s(t)$	burst signal
s_n	n th sampling value of $s(t)$
S_n	n th sampling value of the discrete Fourier transform of $s(t)$
σ	width of the Gaussian function
t	time
T_0	period of a Doppler burst
τ	maximum position of the Gaussian function
τ_1, τ_2	estimated maximum position of burst 1 or burst 2
Θ	angle of beam intersection

7 References

- [1] *K. Bauckhage*: The Phase-Doppler-Difference-Method, a New-Laser-Doppler Technique for Simultaneous Size and Velocity Measurement—Part 1: Description of the Method. Part. Part. Syst. Charact. 5 (1988) 16–22.
- [2] *K. Bauckhage, H.-H. Flögel, U. Fritsching, R. Hiller*: The Phase-Doppler-Difference-Method, a New-Laser-Doppler Technique for Simultaneous Size and Velocity Measurement—Part 2: Optical Particle Characteristics as a Base for the New Diagnostic Technique. Part. Part. Syst. Charact. 5 (1988) 66–71.
- [3] *M. Borys*: Informationsverarbeitung für Teilchengrößeneßplätze nach dem Phasendifferenz- bzw. Impulsverschiebungsverfahren. Diplomarbeit, Universität Rostock, Sektion Technische Elektronik, 1991.
- [4] *P. F. Filtchikow*: Numerische und graphische Methoden der angewandten Mathematik. Vieweg, Braunschweig 1975.
- [5] *K. Hishida, K. Kobashi, M. Maeda*: Improvement of LDA/PDA Using a Digital Signal Processor (DSP). Proc. 3rd Int. Conf. on Laser Anemometry—Advances and Applications. Swansea, 1989.
- [6] *K. Kafadar*: Gaussian White-Noise Generation for Digital Signal Synthesis. IEEE Trans. Instrum. Meas. 35 (1986) 492–495.
- [7] *L. Lading*: Spectral Analysis Versus Counting. Proc. Int. Symp. on Laser Anemometry, ASME 33 (1985) 189–196.
- [8] *A. Oppenheim, R. W. Schäfer*: Discrete-time signal processing. Prentice Hall, Englewood Cliffs, NJ 1989.
- [9] *S. K. Park, K. W. Miller*: Random Number Generators: Good Ones Are Hard to Find. Commun. ACM 31 (1988) 1192–1201.
- [10] *M. Saffman, P. Buchhave, H. Tanger*: Simultaneous Measurement of Size, Concentration and Velocity of Spherical Particles by a Laser Doppler Method. Proc. 2nd Int. Symp. on Appl. of Laser Anemometry to Fluid Mech. Lisbon, July 1984.
- [11] *E. H. Schombacher, T. Wriedt, K. Bauckhage*: Sizing of Droplets Within Liquid Mediums. Proc. Partec 95–4th International Congress Optical Particle Sizing, Nürnberg 1995 pp. 519–528.
- [12] *K. A. Shinpaugh, R. L. Simpson, A. L. Wicks, S. M. Ha, J. L. Fleming*: Signal-Processing Techniques for Low Signal-to-Noise Ratio Laser Doppler Velocimetry Signals. Exp. Fluids 12 (1992) 319–328.
- [13] *H. Tan, J. Loh*: Real-Time Laser Doppler and Phase Doppler Signal Processors. Opt. Lasers Eng. 17 (1992) 229–240.
- [14] *C. Tropea, G. Dimacek*: Evaluation of the Burst Spectrum Analyser LDA Signal Processor. Proc. Int. Symp. on Appl. of Laser Anemometry to Fluid Mech., Lisbon 1988.
- [15] *C. Tropea, T.-H. Xu, F. Onofri, G. Gréhan, P. Haugen, M. Stieglmeier*: Dual Mode Phase Doppler Anemometer. Proc. Partec 95–4th International Congress Optical Particle Sizing, Nürnberg 1995, pp. 287–296.
- [16] *T. Wriedt, K. Bauckhage, A. Schöne*: Application of Fourier Analysis to Phase Doppler Signals Generated by Rough Metal Particles. IEEE Trans. Instrum. Meas. 38 (1989) 984–990.